



**HAL**  
open science

## Innovative combination of spectroscopic techniques to reveal nanoparticle fate in a crop plant

Camille Larue, Hiram Castillo-Michel, Ricardo Stein, Barbara Fayard, Emeline Pouyet, Julie Villanova, Valérie Magnin, Ana-Elena Pradas del Real, Nicolas Trcera, Samuel Legros, et al.

► **To cite this version:**

Camille Larue, Hiram Castillo-Michel, Ricardo Stein, Barbara Fayard, Emeline Pouyet, et al.. Innovative combination of spectroscopic techniques to reveal nanoparticle fate in a crop plant. *Spectrochimica Acta Part B: Atomic Spectroscopy*, 2016, 119, pp.17-24. 10.1016/j.sab.2016.03.005 . hal-02325166

**HAL Id: hal-02325166**

**<https://hal.science/hal-02325166v1>**

Submitted on 10 Nov 2020

**HAL** is a multi-disciplinary open access archive for the deposit and dissemination of scientific research documents, whether they are published or not. The documents may come from teaching and research institutions in France or abroad, or from public or private research centers.

L'archive ouverte pluridisciplinaire **HAL**, est destinée au dépôt et à la diffusion de documents scientifiques de niveau recherche, publiés ou non, émanant des établissements d'enseignement et de recherche français ou étrangers, des laboratoires publics ou privés.

1 **Innovative combination of spectroscopic techniques to reveal nanoparticle fate in a crop plant**

2 Camille Larue<sup>a\*</sup>, Hiram Castillo-Michel<sup>b</sup>, Ricardo J. Stein<sup>c</sup>, Barbara Fayard<sup>d,e</sup>, Emeline Pouyet<sup>b</sup>, Julie  
3 Villanova<sup>f</sup>, Valérie Magnin<sup>a</sup>, Ana-Elena Pradas del Real<sup>a</sup>, Nicolas Trcera<sup>g</sup>, Samuel Legros<sup>h</sup>, Stéphanie  
4 Sorieul<sup>i</sup>, Géraldine Sarret<sup>a</sup>

5  
6 <sup>a</sup>ISTerre, Université Grenoble Alpes, CNRS, F-38041 Grenoble, France. [camille.larue@ensat.fr](mailto:camille.larue@ensat.fr),  
7 [valerie.magnin@univ-grenoble-alpes.fr](mailto:valerie.magnin@univ-grenoble-alpes.fr), [geraldine.sarret@univ-grenoble-alpes.fr](mailto:geraldine.sarret@univ-grenoble-alpes.fr), [ana.pradas@univ-  
grenoble-alpes.fr](mailto:ana.pradas@univ-<br/>8 grenoble-alpes.fr)

9 <sup>b</sup>ESRF, beamline ID21, Grenoble, France. [castillo@esrf.fr](mailto:castillo@esrf.fr), [emeline.pouyet@esrf.fr](mailto:emeline.pouyet@esrf.fr)

10 <sup>c</sup>Department of Plant Physiology, Ruhr University Bochum, Universitätsstrasse 150, 44801 Bochum,  
11 Germany. [ricardo.stein@rub.de](mailto:ricardo.stein@rub.de)

12 <sup>d</sup>LPS CNRS UMR 8502 - Université Paris Sud Bât 510 - F-91405 Orsay cedex.

13 <sup>e</sup>Actual adress : Novitom - 1, place Firmin Gautier -F-38000 Grenoble. [barbara.fayard@novitom.com](mailto:barbara.fayard@novitom.com)

14 <sup>f</sup>ID16B, ESRF - The European synchrotron, CS40220 38043 Grenoble Cedex 9, France.  
15 [julie.villanova@esrf.fr](mailto:julie.villanova@esrf.fr)

16 <sup>g</sup>Synchrotron SOLEIL, Gif-sur-Yvette F-91192, France. [nicolas.trcera@synchrotron-soleil.fr](mailto:nicolas.trcera@synchrotron-soleil.fr)

17 <sup>h</sup>CEA/LITEN/DTNM/L2T, CEA Grenoble, Av des Martyrs, 38054 Grenoble Cedex 9, France.  
18 [samuel.legros@cirad.fr](mailto:samuel.legros@cirad.fr)

19 <sup>i</sup>Université Bordeaux, CNRS/IN2P3, Centre d'Etudes Nucléaires de Bordeaux Gradignan, CENBG,  
20 Chemin du Solarium, BP120, 33175 Gradignan, France. [sorieul@cenbg.in2p3.fr](mailto:sorieul@cenbg.in2p3.fr)

21

22

23 \* corresponding author : [camille.larue@ensat.fr](mailto:camille.larue@ensat.fr)

24 Present address: CNRS; EcoLab; 31326 Castanet Tolosan, France

25 **Abstract**

26 Nanotechnology is the new industrial revolution of our century. Its development leads to an increasing  
27 use of nanoparticles and thus to their dissemination. Their fate in the environment is of great concern  
28 and especially their possible transfer in trophic chains might be an issue for food safety. However, so  
29 far our knowledge on this topic has been restricted by the lack of appropriate techniques to  
30 characterize their behavior in complex matrixes. Here, we present in detail the use of cutting-edge  
31 beam-based techniques for nanoparticle *in situ* localization, quantification and speciation in a crop  
32 plant species (*Lactuca sativa*). Lettuce seedlings have been exposed to TiO<sub>2</sub> and Ag nanoparticles and  
33 analyzed by inductively coupled plasma spectrometry, micro particle induced X-ray emission coupled  
34 to Rutherford backscattering spectroscopy on nuclear microprobe, micro X-ray fluorescence  
35 spectroscopy and X-ray absorption near edge structure spectroscopy. The benefits and drawbacks of  
36 each technique are discussed, and the type of information that can be drawn, for example on the  
37 translocation to edible parts, change of speciation within the plant, detoxification mechanisms, or  
38 impact on the plant ionome, are highlighted. Such type of coupled approach would be an asset for  
39 nanoparticle risk assessment.

40

41

42

43

44

45 **Keywords:** nanoparticle; micro X-ray fluorescence spectroscopy; X-ray absorption near edge  
46 spectroscopy; micro-particle induce X-ray emission/Rutherford backscattering spectroscopy;  
47 multivariate statistical analysis

48

## 49        **1. Introduction**

50        Nanotechnologies are developing fast with increasing number of applications in fields like medicine,  
51        sustainable development or plant protection products. They represent promising solutions to current  
52        issues such as more efficient disease treatment on targeted organs or decreased inputs of pesticides  
53        in the environment [1]. These new applications also imply an increased dissemination of nanoparticles  
54        (NPs, particles with at least one dimension below 100 nm) in ecosystems. Still, their fate in the  
55        environment is largely unknown mainly because of the lack of adapted techniques to assess their  
56        behavior in complex matrices (soil, plant or animal).

57        Two types of complementary techniques can be used to investigate the fate of NPs: bulk and imaging  
58        techniques. The most often used technique for the quantification of metallic NP on bulk samples is  
59        inductively coupled plasma – mass or atomic emission spectrometers (ICP-MS, ICP-AES) [7–9].

60        Although ICP techniques have very low detection limits (down to  $\text{ng}\cdot\text{kg}^{-1}$  [10]), and provide an essential  
61        information, they cannot provide spatial information. Thus, in the case of plant roots, they average  
62        adsorbed and absorbed elements from different tissue layers which can result in distorted data.

63        Sample preparation can be an issue if proper acidic digestion of NPs has not been established. Often,  
64        standard digestion protocols do not take into account the particulate form of NPs, which may render  
65        them less soluble, and thus can lead to underestimation of NP content. Localizing NPs inside biological

66        tissues requires 2D techniques such as scanning and transmission electron microscopy (SEM, TEM)  
67        coupled with an energy dispersive X-ray spectrometer (EDS) [2–4]. SEM is often used to investigate the  
68        fate of NPs on organism surface (for instance to visualize carbon nanotubes sticking out of root  
69        epidermis [5]) or on cross-sections but has a low sensitivity (detection limit around  $1000 \text{ mg}\cdot\text{kg}^{-1}$  [6]).

70        TEM has a very good lateral resolution allowing investigations at the cellular to sub-cellular scale, but  
71        it is not suited for localization of metal at the organ scale. More important, sample preparation (water  
72        substitution, resin embedding, staining, coating) can generate artifacts and elemental relocation.

73        Existing cryotechniques (high pressure freezing, cryosubstitution) are highly valuable, but not  
74        commonly used in this field. These technical limitations represent a major bottleneck to advance our

75 understanding of NP fate in the environment.

76 To overcome these issues, the combination of both bulk analyses and 2D techniques is a powerful  
77 approach. In particular, micro beam-based techniques are useful but underused tools in biology [11–  
78 13]. These techniques are based on - but not restricted to - synchrotron radiation (photon) or ion  
79 (proton) beams. On synchrotron, elemental distribution can be studied by micro-X-ray fluorescence  
80 ( $\mu$ XRF) and chemical state by X-ray absorption near edge structure spectroscopy using a micro-focused  
81 beam ( $\mu$ XANES) or in full-field mode. On nuclear microprobes, metal distribution and *in situ*  
82 quantification can be obtained by combining micro-particle induced X-ray emission ( $\mu$ PIXE) and  
83 Rutherford backscattering spectroscopy ( $\mu$ RBS). These techniques are already well-known and widely  
84 used in chemistry, physics or material science but their development in biology and environmental  
85 sciences is more recent [12,13]. Latest developments in sample environment, detector sensitivity and  
86 spatial resolution had allowed their use for biological samples.

87 In this study, we report the complementarity of chosen beam-based techniques to determine the fate  
88 of two different types of NPs in a crop plant: lettuce (*Lactuca sativa*). Plants are a major component of  
89 ecosystems: they are at the interface between air, water and soil and at the base of the human food  
90 chain. We chose to study the behavior of two metal-containing NPs widely produced[1]: titanium  
91 dioxide ( $\text{TiO}_2$ ) and silver (Ag) NPs. Moreover, these NPs have also been selected for their contrasted  
92 solubilities [14].

93 Lettuce seedlings were exposed in hydroponics to different concentrations of  $\text{TiO}_2$  and Ag-NPs. After 7  
94 days, plantlets were analyzed by a combination of techniques: ICP-MS and ICP-AES,  $\mu$ PIXE/RBS,  $\mu$ XRF  
95 and XANES. Emphasis has also been settled on sample preparation for the different techniques  
96 (optimization of the digestion procedure, preparation and observation of samples in cryogenic  
97 conditions). This innovative approach permitted to deepen our knowledge about NP fate in plants and  
98 to obtain original data about their impact on plant ionome.

99

## 100 **2. Material and Methods**

101 **2.1. Plant culture & NP characterization**

102 Lettuce seeds (*Lactuca sativa*, var. Laitue Romaine) were exposed for one week to 0, 10, 100, 1000  
103 mg.L<sup>-1</sup> Ag or TiO<sub>2</sub>-NPs in a modified Hoagland solution. Those concentrations are representative of an  
104 acute contamination of the environment [15] and permitted to test the detection limits of the  
105 employed techniques. Uncoated Ag (≈ 40 nm) and TiO<sub>2</sub> (anatase, 4 nm) NPs were used. An Ag<sup>+</sup> exposure  
106 condition was also set-up to account for Ag-NP dissolution. More details on plant culture and NP  
107 characterization are available in the supplementary data and Figure S1 (Appendix).

108

109 **2.2. Metal quantification by ICP-AES and ICP-MS**

110 Usual digestion protocols (using hot HNO<sub>3</sub>) might not be stringent enough to mineralize NPs as well as  
111 plant tissues, leading to the underestimation of metal concentrations. To obtain reliable data, effort  
112 was put to find out the best digestion protocol for both types of NPs testing the influence of several  
113 parameters (temperatures, type of acids, ratio NP powder/acid volume). Ag-NPs were easily  
114 mineralized regardless of the chemicals and the temperature conditions used. The following protocol,  
115 which was also efficient to mineralize plant tissue (white cabbage), was chosen: 1 mL HNO<sub>3</sub>, 1.5 mL  
116 HClO<sub>4</sub> at 70°C during 24 h. For TiO<sub>2</sub>-NPs, we chose a microwave assisted digestion using 5 ml H<sub>2</sub>SO<sub>4</sub>, 3  
117 ml of HNO<sub>3</sub> and 1 ml of H<sub>2</sub>O<sub>2</sub>. Digestion yields of the different protocols are gathered in Table S1  
118 (Appendix). Roots of three individuals per conditions were harvested, weighted and analysed for Ti  
119 and Ag concentrations on an ICP-AES for Ag-NPs and using an ICP-MS for TiO<sub>2</sub>-NPs. More details are  
120 available in the supplementary data (Appendix).

121

122 **2.3. Sample preparation for beam-based techniques**

123 Beam-based techniques permit to have access to localized information. Sample preparation is a crucial  
124 step and if not properly done can lead to redistributions and changes in the speciation of elements  
125 [16]. To prevent this, samples were prepared under cryogenic conditions. First, roots and stems were  
126 thoroughly washed with deionized water to take off NPs lightly bound to the surface. Then samples

127 were cut in small pieces (2 mm) and immersed in a droplet of resin (Tissue Teck Sakura) and  
128 immediately cryo-fixed by plunging the sample in isopentane cooled with liquid nitrogen. The small  
129 size of the sample and droplet of resin allows rapid freezing of the whole tissue. Finally, samples were  
130 cut in thin cross-sections (20  $\mu\text{m}$ ) using a cryo-microtome (Leica). Cross-sections were mounted on  
131 appropriate sample holder for synchrotron experiments or freeze-dried (48h,  $-52^{\circ}\text{C}$ , 0.01 mbars) for  
132 nuclear microprobe and XANES full-field analyses.

133

#### 134 **2.4. Proton beam-based techniques – *In situ* quantification by $\mu\text{PIXE/RBS}$**

135 Samples (prepared as specified in 2.3) were analyzed in freeze-dried state under vacuum on the AIFIRA  
136 nuclear microprobe [17]. For this experiment, beamline was operated with a proton source at 3 MeV  
137 with a beam focused to 2.5  $\mu\text{m}$  and a current intensity of 500 pA. Mapping of low-Z elements (H, C, N  
138 and O) was performed using RBS, in parallel with PIXE for the quantification of elements heavier than  
139 Mg. Detection limit is around 100  $\mu\text{g.g}^{-1}$ . Data processing was performed using several softwares:  
140 Supavisio [18], SIMNRA [19] and GUPIX [20]. More details are available in the supplementary data  
141 (Appendix).

142

#### 143 **2.5. Synchrotron based techniques – Distribution by $\mu\text{XRF}$ and chemical speciation by XANES**

144 Synchrotron experiments were carried out on three beamlines: ID21 [21] and ID22 [22] at the  
145 European Synchrotron Radiation Facility (ESRF, Grenoble, France) and LUCIA at SOLEIL (Saint Aubain,  
146 France).

147 To avoid beam damage, acquisitions were performed under cryogenic conditions on ID21 and LUCIA.  
148  $\mu\text{XRF}$  maps were recorded with various step sizes (from 0.1 to 3  $\mu\text{m}$ ) with a dwell time from 100 to  
149 2000 ms.  $\mu\text{XRF}$  data were fitted using PyMCA software [23].

150 Ag  $L_{III}$ -edge (3.33 to 3.45 keV energy range, 0.5 eV step) and Ti-K edge (4.96 to 5.05 keV energy range,  
151 0.5 eV step)  $\mu\text{XANES}$  spectra were recorded in regions of interest of the fluorescence maps. The beam  
152 position was slightly moved from one spectrum to another to avoid radiation damage. At least 10

153 spectra of 30s were averaged for each point of interest, after checking the absence of radiation  
154 damage. XANES spectra on reference compounds were recorded during previous experiments [24,25]  
155 (Figure S2, Appendix).

156 Full-field measurements were performed at the ID21 XANES full-field end-station [26]. The achievable  
157 pixel size is 0.32  $\mu\text{m}$ . Measurements were recorded on freeze-dried samples using the Si(111)  
158 monochromator with an energy step of 0.3 eV from 3.33 to 3.42 keV for Ag L-edge; and Si(220) with  
159 an energy step of 0.3 eV from 4.95 to 4.98 keV and 1 eV from 4.98 to 5.06 keV for Ti K-edge. Data  
160 processing was made using the SIFT\_PyOCL procedure [27] and TXM-Wizard [28].

161 XANES data treatment was performed using Athena software [29] according to Larue *et al.* [24,25].

162 More details are available in the supplementary data (Appendix).

163

## 164 **2.6. Statistical analysis**

165 To achieve normality and homoscedasticity, data were  $\log_{10}$  transformed. They were compared using  
166 one-way ANOVA (for Ti and Ag concentrations in roots as measured by ICP) or two-way ANOVA (for  
167 plant fresh biomass), with organ (roots or leaves) and treatment (control,  $\text{TiO}_2$ -NPs, Ag ionic and Ag-  
168 NPs) as main effects, and the interaction (organ x treatment). Post hoc tests (pairwise T-tests with  
169 Bonferroni correction, and Tukey tests) were applied to detect differences between groups of samples.  
170 Differences were considered significant when  $p \leq 0.05$ .

171 To analyze  $\mu\text{PIXE/RBS}$  quantitative results and the effect of the different NP concentrations on the root  
172 (divided in epidermis, parenchyma and vascular cylinder) ionome (comprising Ca, Cl, Cu, Fe, K, Mn, Mg,  
173 Na, P, S, Si and Zn concentrations) we used linear discriminant analysis (LDA) and principal component  
174 analysis (PCA). Those techniques are known as part of a group of exploratory data analyses which  
175 permit to accommodate the small number of biological replicates due to beamtime restrictions. Data  
176 were first  $\log_{10(+1)}$  transformed, then standardized. For LDA, the homogeneity between within-group  
177 covariance matrices were tested *prior* the analysis.



178 All statistical analyses were performed using the R statistical software [30], with the vegan [31] and  
179 MASS [32] packages.

180

181

### 182 **3. RESULTS and DISCUSSION**

#### 183 **3.1. Toxicity symptoms and ICP metal concentrations**

184 Exposure to the highest NP concentration (1000 mg.L<sup>-1</sup>) affected the plant fresh weight ( $F=3.48$ ,  
185  $P=0.041$ ), but no interaction between NP treatment and organs could be detected ( $F=0.90$ ,  $P=0.46$ ),  
186 indicating that both roots and leaves were affected similarly by the exposure to NPs (Figure S3A,  
187 Appendix). Plants showed reduced fresh weight in roots and leaves when exposed to Ag-NPs (roots:  
188  $176.60 \pm 78.78$  mg; leaves:  $1165.87 \pm 350.73$  mg) and Ag<sup>+</sup> (roots:  $150.97 \pm 54.30$  mg; leaves:  $1172.70 \pm$   
189  $625.73$  mg) in comparison to control (roots:  $349.83 \pm 121.82$  mg; leaves:  $1312.70 \pm 328.77$  mg) and  
190 TiO<sub>2</sub>-NP treated plants (roots:  $322.67 \pm 95.54$  mg; leaves:  $1586.63 \pm 433.67$  mg). Plants exposed to Ag  
191 (ions and NPs) were displaying early senescence signs and brownish roots (Figure S3B, Appendix).

192 These results are consistent with previous studies on various plants reporting no acute phytotoxicity  
193 symptoms following TiO<sub>2</sub>-NP exposure [33–37] but decreased root length and biomass after Ag-NP  
194 treatment for rice [38] or ryegrass [39]. A study published on the comparative effect of Ag-NPs vs. TiO<sub>2</sub>-  
195 NPs on tomato also highlighted different phytotoxicity profiles [40]. It is also interesting to notice that  
196 the condition accounting for Ag-NP dissolution led to the same growth inhibition that the Ag-NP  
197 condition itself. It brings to light the usual question dealing with Ag-NP toxicity: does it come from the  
198 NPs or from the dissolution of Ag<sup>+</sup> ions? According to several studies Ag as ions would be more toxic  
199 than Ag as NPs [41–43]. However, NP toxicity would come for a large part from the release of Ag ions  
200 during exposure but the nanoparticulate form would also play a specific role in the phytotoxicity  
201 process: negatively charged NPs might diffuse more easily than cations within organic matrices [43],  
202 and internalized Ag-NPs might then release Ag<sup>+</sup> inside the biological compartments [44–46]. Within  
203 the framework of our experiment (high Ag concentrations, short-term exposure), our results rather

204 support the hypothesis of toxicity coming primarily from Ag ions. This conclusion is in good agreement  
205 with a study showing that, if the soluble Ag fraction is high, NPs will not add measurable additional  
206 toxicity but at low Ag ionic fraction the nanoparticulate form will increase the phytotoxicity [44].  
207 After exposure, metal concentrations in plants were assessed by ICP-AES and ICP-MS. Roots of control  
208 seedlings contained low level of both metals (Ti and Ag < 6 mg.kg<sup>-1</sup>). After a 7-day exposure to 1000  
209 mg.L<sup>-1</sup> NPs, it was significantly higher: 238.0 ± 54.9 (F=128.2, P=1.2.10<sup>-5</sup>) and 1600.5 ± 271.3 (F=49.42,  
210 P=0.002) mg.kg<sup>-1</sup> fresh weight (FW) of Ag and Ti respectively (Figure S4, Appendix).  
211 Ti root concentration was more than 6 times higher than Ag root concentration when exposed to the  
212 same initial NP concentration. This trend was not seen in the other comparative study between Ag and  
213 TiO<sub>2</sub>-NPs on tomato in which Ag concentration in roots was higher [40]. This difference could be linked  
214 to the difference in exposure media. Tomato seedlings were exposed in ultrapure water and lettuces  
215 in this study in Hoagland solution; this will impact NP behaviour in suspension (agglomeration and  
216 dissolution) and thus their interaction with plants. Moreover, different species might also have  
217 different uptake as suggested by a study comparing Ti uptake in wheat, common bean and curly dock  
218 [34] showing root concentration ranging from 2460 to 5280 mg.kg<sup>-1</sup>. Additionally, no information is  
219 available on the digestion protocol used for ICP measurements so direct comparison might not be  
220 pertinent (Table S1, Appendix). Another interesting fact is that the same growth inhibition of the two  
221 Ag treatments noticed before (Figure S3, Appendix) is not linked to similar Ag concentrations in lettuce  
222 roots. Ag concentration in roots of seedlings exposed to Ag<sup>+</sup> was significantly lower (82.3 ± 5.2 mg.kg<sup>-1</sup>  
223 FW, F=128.2, p=1.2.10<sup>-5</sup>) than in plants exposed to Ag-NPs (Figure S3A, Appendix). This result suggests  
224 that not only Ag<sup>+</sup> ions first dissolved from NPs in the medium are taken up by lettuce roots. Several  
225 hypotheses can be proposed: (i) either NPs can penetrate plant roots creating “channels” (as it has  
226 been suggested for carbon nanotubes and tomato seed coat [47]) that will facilitate other ion/NP  
227 internalisation and internalized NPs would release ions directly into cells [46], or (ii) NP interaction  
228 with the root surface enhances their dissolution at the vicinity of the root and subsequently the uptake

229 of Ag<sup>+</sup> [39,42] with possible later Ag reduction inside organisms [48], or (iii) a large part of NPs and  
230 their secondary products are sorbed on the root surface.

231 Finally, these ICP measurements suggest that there is no apparent link between toxicity symptoms  
232 (more toxicity for Ag) and metal accumulation in roots (more Ti accumulated).

233 However, ICP-AES and ICP-MS provide bulk analyses and do not distinguish between metal adsorbed  
234 on the root surface vs. internalized inside the roots. To shed light on this aspect, a spatially resolved  
235 and quantitative approach is needed.

236

### 237 **3.2. *In situ* quantification by $\mu$ PIXE/RBS**

238 Lettuce roots were exposed to Ag<sup>+</sup> (10 mg.L<sup>-1</sup>), Ag-NPs and TiO<sub>2</sub>-NPs (10 to 1000 mg.L<sup>-1</sup>); root and stem  
239 cross-sections were imaged by  $\mu$ PIXE (Figure S5 - Appendix, Table 1). The Ag<sup>+</sup> treatment lead to  
240 undetectable level of Ag using this technique and was discarded from the analysis.  $\mu$ RBS analysis in  
241 parallel made it possible to obtain reliable local quantification by area of interest in the samples (Figure  
242 S5, S6 - Appendix). Differently to ICP-AES/ICP-MS analyses, results are expressed in mg.kg<sup>-1</sup> dry weight  
243 (DW). For rough estimation, one could consider 10% of dry matter for lettuce roots.

244 Considering results averaged on the whole cross-section including the root surface,  $\mu$ PIXE/RBS and ICP-  
245 AES/ICP-MS results are in good agreement, evidencing a different behavior between the TiO<sub>2</sub> and Ag  
246 NPs (Figure S6, Appendix). In the analyzed cross-sections, Ti was 12 times more concentrated than Ag:  
247 25390 and 2096 mg.kg<sup>-1</sup> DW respectively after the 1000 mg.L<sup>-1</sup> treatment. The difference between Ti  
248 and Ag concentration at the cross-section scale is due to a high Ti adsorption on root epidermis in  
249 comparison with the parenchymal concentration (for Ti p<0.05, for Ag p=0.26): 71455  $\pm$  10083 mg  
250 Ti.kg<sup>-1</sup> in the epidermis area vs. 5888  $\pm$  5670 mg Ag.kg<sup>-1</sup>. So using a 2D mapping technique and focusing  
251 on the contribution of each tissue type (epidermis vs. parenchyma vs. vascular cylinder), the conclusion  
252 is different. If the epidermis area is discarded, one can conclude that lettuce root had taken up more  
253 Ag than Ti with approximately 878  $\pm$  399 mg Ag.kg<sup>-1</sup> DW contained in the parenchyma and vascular  
254 cylinder compared to 99  $\pm$  89 mg.kg<sup>-1</sup> DW for Ti (Figure S6, Appendix). This phenomenon was also

255 suggested to explain the high Ti concentration in *Vicia faba* [35], bean [34], wheat [34,36] and rapeseed  
256 [37]. In terms of risk assessment, these  $\mu$ PIXE/RBS results suggest that Ag is more worrying since it is  
257 taken up by lettuce roots in higher amount and thus is more susceptible to translocate towards the  
258 edible parts. Inversely, Ti is found aggregated at the root surface but a small amount is internalized. If  
259 one had only considered ICP-AES/ICP-MS data, the conclusion would have been the reverse.

260 The leaves were not analyzed by ICP-AES, but stem cross-sections for the plants exposed to 1000 mg.L<sup>-1</sup>  
261 were analyzed by  $\mu$ PIXE to identify a possible translocation of Ag and Ti towards the leaves (Figure  
262 S6, Appendix). Ti was detected in all stem tissues: epidermis:  $283 \pm 292$  mg.kg<sup>-1</sup>, parenchyma:  $27 \pm 15$   
263 mg.kg<sup>-1</sup> and vascular cylinder:  $48 \pm 39$  mg.kg<sup>-1</sup>. Its distribution was uneven with for instance a hot spot  
264 of Ti in the stem vascular cylinder at 2254 mg.kg<sup>-1</sup> DW and high variations within replicates. Ag was not  
265 detected in the stem even if its concentration in roots was higher than Ti concentration. An explanation  
266 to this phenomenon could be the chemical form of the detected element. If Ag is dissolved inside  
267 plants then Ag ions would be more mobile and distributed homogeneously in plant tissue leading to a  
268 low local Ag concentration, below detection limit. Inversely, Ti due to its limited dissolution would  
269 remain as NPs and form hot spots of aggregated NPs thus reaching locally the detection limit of  $\mu$ PIXE  
270 technique.

271 To evaluate the most appropriate exposure condition for this type of experiment, plants were also  
272 exposed to 10 and 100 mg.L<sup>-1</sup> TiO<sub>2</sub> and Ag-NPs. At 100 mg.L<sup>-1</sup> Ag was still detectable in the parenchyma  
273 of lettuce roots with approximately the same concentrations as when exposed to 1000 mg.L<sup>-1</sup> but was  
274 under detection limits in the vascular cylinder. At the lowest exposure concentration (10 mg.L<sup>-1</sup>), Ag  
275 was always below detection limits. Inversely, Ti was detectable in all used concentrations with the  
276 existence of Ti overaccumulation on root epidermis. This comparison with lower concentrations  
277 confirms results obtained at the highest concentration and also validates our hypothesis of the lower  
278 detectability of Ag in comparison to Ti. Even if Ag is more taken up by lettuce than Ti, it becomes under  
279 detection limit for lower doses whereas Ti is still detectable.

280 Interestingly, there was no significant difference in Ti concentrations between the 100 and the 1000  
281 mg.L<sup>-1</sup> treatments (p=0.96). This can be explained by the higher accumulation of Ti at the root surface  
282 in the 1000 mg.L<sup>-1</sup> exposure which might act as a physical barrier limiting the diffusion and uptake of  
283 Ti inside the root tissues (lower Ti concentration in both the parenchyma and vascular cylinder). This  
284 effect was not visible for Ag-NP exposure in which concentrations in the tissues increased with Ag  
285 exposure (p=5.73.10<sup>-9</sup>).

286 A question arising from the high accumulation of Ti on the root surface is its potential influence on  
287 plant ionome [49]. Very little has been done so far to investigate the impact of NP exposure on plant  
288 nutrition (*Elodea Canadensis* [34], *Arabidopsis thaliana* [50]) and presently there is no study on crop  
289 plants. A major advantage of  $\mu$ PIXE is the possibility to access the distribution of all elements  
290 permitting the identification of co-localizations or changes in elemental concentrations.

291 To analyze the effect of different NP concentrations on the elemental accumulation in roots, we used  
292 multivariate statistics analysis techniques, namely LDA and PCA. Both techniques are widely used in  
293 multivariate statistics [51], LDA being applied to discriminate classes of data, and PCA to identify  
294 relationships between variables, without taking into account classes or structures in the data. Across  
295 all conditions (NP concentrations and plant tissues), a clear discrimination (LD1: 0.8086) between the  
296 control and NP-exposed roots could be detected by LDA (Figure 1A), with Cu (eigenvalue=2.53, Ctrl: 202  
297 mg.kg<sup>-1</sup>, Ag-NP: 39 mg.kg<sup>-1</sup>, TiO<sub>2</sub>-NP: 42 mg.kg<sup>-1</sup>), Fe (eigenvalue=-1.96, Ctrl: 22 mg.kg<sup>-1</sup>, Ag-NP: 38 mg.kg<sup>-1</sup>,  
298 TiO<sub>2</sub>-NP: 40 mg.kg<sup>-1</sup>), Mn (eigenvalue=1.50, Ctrl: 195 mg.kg<sup>-1</sup>, Ag-NP: 25 mg.kg<sup>-1</sup>, TiO<sub>2</sub>-NP: 59 mg.kg<sup>-1</sup>)  
299 and Ca (eigenvalue=-1.30, Ctrl: 9923 mg.kg<sup>-1</sup>, Ag-NP: 22374 mg.kg<sup>-1</sup>, TiO<sub>2</sub>-NP: 213482 mg.kg<sup>-1</sup>) being  
300 among the most important elements for the discrimination of the groups on the first discriminant axis.

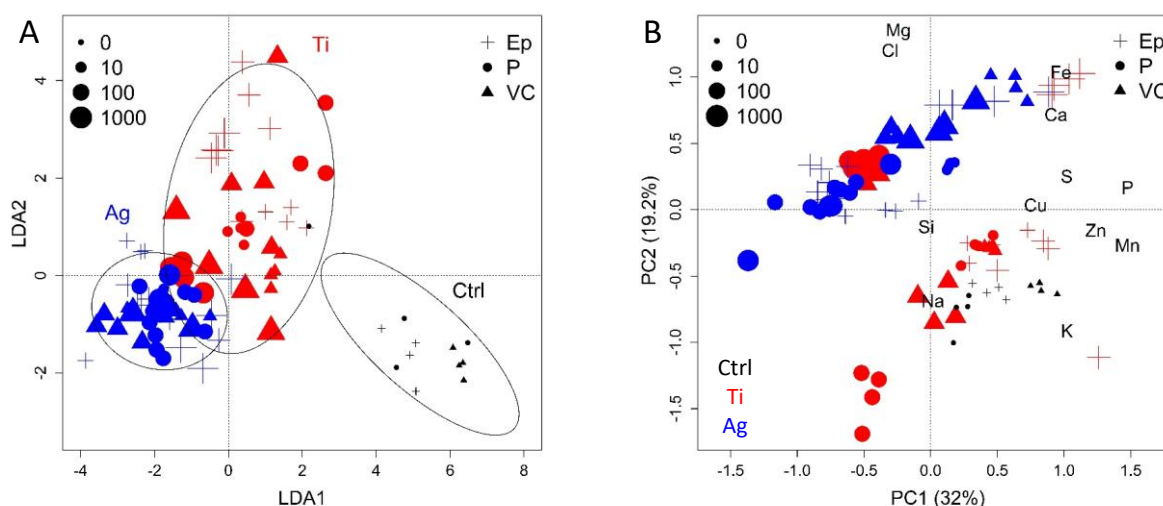
301 A less clear discrimination between the Ag and TiO<sub>2</sub> treatments could be detected (as seen by the  
302 partial overlap of the 90% tolerance intervals in Figure 1A), indicating a possible common effect of both  
303 NPs on the root elemental concentrations. ICP measurements on *Arabidopsis* exposed to Ag-NPs  
304 showed a decreased concentration for K, Fe and Zn [50]. Though the direct comparison is difficult  
305 because of the very different exposure conditions (2 mg.L<sup>-1</sup> in agar medium vs. 10 to 1000 mg.L<sup>-1</sup> in

306 hydroponics), LDA on lettuce roots also highlighted a disrupted Fe homeostasis with an eigen value of  
307 -1.96 whereas the two other elements (K and Zn) were not modified which suggest a species-  
308 dependent effect.

309 To gain deeper insights on the effects of the different NPs and the relationships between elements, a  
310 PCA was performed (Figure 1B). Overall, exposure to Ag-NPs led to a decrease in the concentration of  
311 several elements (such as Cu, Zn, Mn, P, S and K) indicating a large disruption of the root ionome,  
312 whereas common effect of Ag-NPs and TiO<sub>2</sub>-NPs could be seen but only when plants were exposed to  
313 1000 mg.L<sup>-1</sup>. The highest concentration of TiO<sub>2</sub>-NPs also led to a higher accumulation of Fe, P, S and Ca  
314 in the root epidermis, not seen at the lower concentrations. Those higher concentrations in the  
315 epidermis are correlated with decreased concentrations in both the parenchyma and vascular cylinder  
316 of plants treated with 1000 mg.L<sup>-1</sup> TiO<sub>2</sub>-NPs, leading to a similar profile as to plants exposed to Ag-NPs.  
317 The same analyses were also performed after excluding the epidermis from the data set, to consider  
318 only the internal tissues (Figure S7A, B - Appendix). They provided the same clustering of data, and led  
319 to the same conclusions on the changes in root ionome.

320

321 *Figure 1. Root ionome analyzed by  $\mu$ PIXE/RBS. A. LDA statistical analysis of elemental concentrations in roots. B.*  
322 *PCA statistical analysis of elemental concentrations in roots. Elements included in the analysis are Na, Mg, Si, P,*  
323 *Cl, K, Ca, Mn, Fe, Cu and Zn (Ti and Ag excluded). For the figure in color, the reader is referred to the web version*  
324 *of this article.*



325

326

327 To conclude,  $\mu$ PIXE/RBS experiment evidenced a similar impact of Ag-NPs on plant ionome at all  
 328 exposure concentrations, whereas  $\text{TiO}_2$ -NPs displayed a different impact at very high concentration  
 329 ( $1000 \text{ mg.L}^{-1}$ ) as compared to lower concentrations ( $<100 \text{ mg.L}^{-1}$ ). Even without visible acute toxicity  
 330 symptoms at one week exposure, high concentrations of  $\text{TiO}_2$ -NPs may lead to a long-term toxicity by  
 331 acting as a physical barrier disrupting plant homeostasis.

332

### 333 3.3. Metal speciation by XANES

334 To investigate the influence of metal chemical form in plants on their fate, metal speciation *in situ* was  
 335 determined by XANES. To perform  $\mu$ XANES *in situ*, elemental distribution was first mapped by  
 336 synchrotron radiation based- $\mu$ XRF (Table 1). The detection limit of  $\mu$ XRF is lower than for  $\mu$ PIXE, around  
 337  $1 \mu\text{g.g}^{-1}$  in the tissues [52]. The limit to assure a good XANES data quality is one or two orders of  
 338 magnitude higher. Thus, the highest exposure condition was chosen for synchrotron experiments  
 339 ( $1000 \text{ mg.L}^{-1}$  in the exposure medium). Distribution maps of metals in root and stem cross-sections  
 340 obtained after exposure to  $1000 \text{ mg TiO}_2\text{-NPs.L}^{-1}$  and  $1000 \text{ mg Ag-NPs.L}^{-1}$  are presented in Figure 2.

341  $\mu$ XRF results agreed with  $\mu$ PIXE results, showing a continuous layer of Ti at the root surface associated  
 342 with Ca and P (Figure 2E, F, G, H) which explains the high contribution of Ca and P on the PC1 of the  
 343 previous PCA analysis (Figure 1B). Likewise, hot spots of Ti were detected inside roots, in the

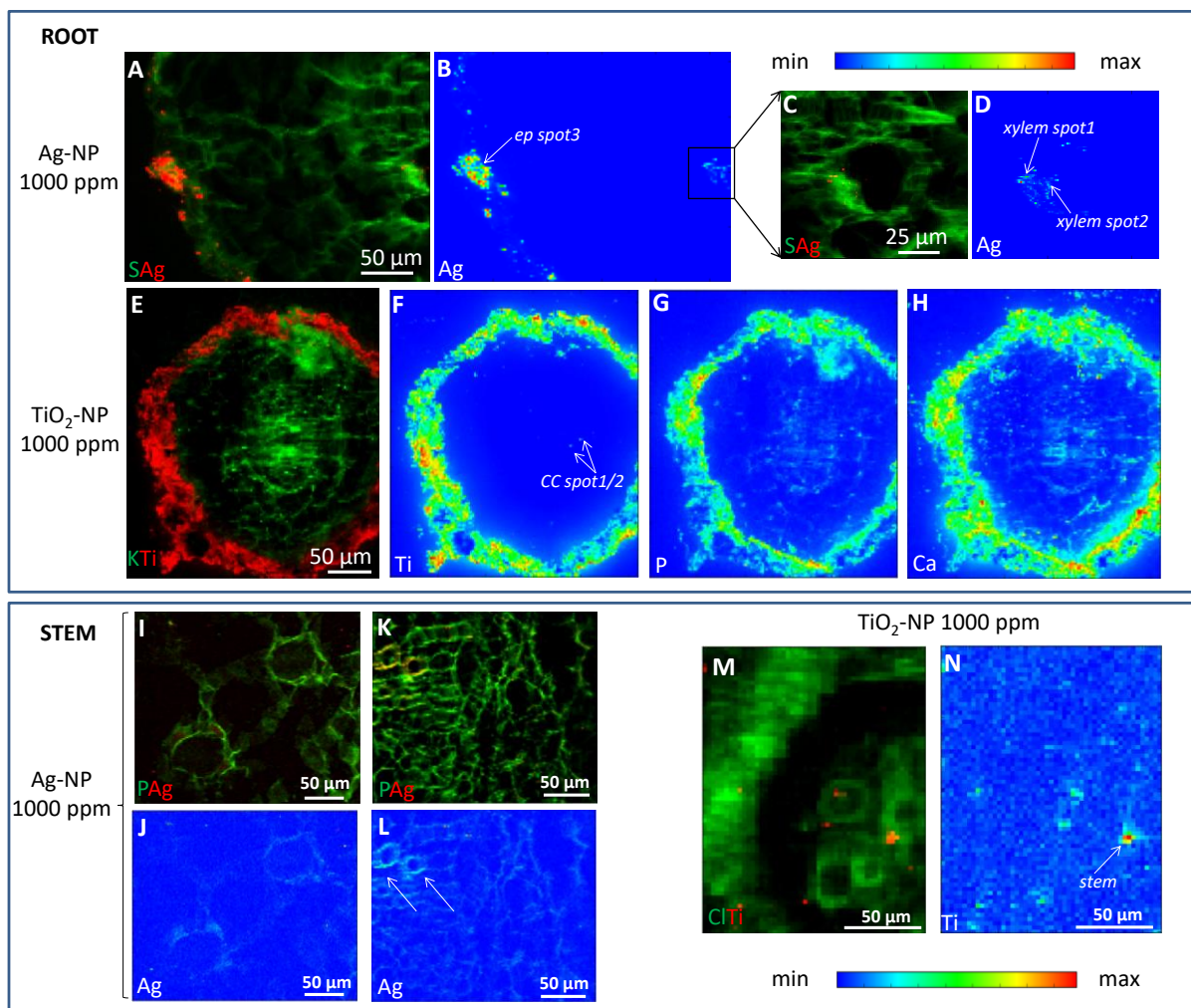
344 parenchyma and in the stem (Figure 2E, F). Ag appeared as agglomerates on root epidermis (Figure 2A,  
345 B). Moreover, the high sensitivity of  $\mu$ XRF also permitted to detect Ag in the root vascular bundle  
346 (Figure 2C, D) as well as in vascular bundles in the stem (Figure 2I, J, K, L). The presence of Ag in the  
347 root vascular cylinder was further confirmed by  $\mu$ XRF analysis of a freeze-dried root cross-section at  
348 the hard X-ray nanoprobe beamline ID22 (excitation at 29.5 KeV, above Ag K-edge) (Table 1, Figure  
349 S8A, B – Appendix). Exciting above the Ag K-edge enhances the sensitivity for Ag due to the higher  
350 fluorescence yield of the K emission lines together with the higher photon flux provided at this  
351 beamline. However at this high energy other relevant elements such S, P, Cl, K and Ca are poorly  
352 detected. These data support the hypothesis that Ag-NPs were transferred through the vascular  
353 system to the edible tissue of lettuces. For  $\text{TiO}_2$ -NPs the conclusion needs to be mitigated since this Ti  
354 also exists as a geogenic element in earth crust. Translocation of both  $\text{TiO}_2$  and Ag-NPs in other plant  
355 species and transfer to edible parts of crops including cucumber [53,54], tomato [40] and rice [38] have  
356 already been demonstrated.

357

358 *Figure 2.  $\mu$ XRF analysis of lettuce roots and stems exposed for 7 days in hydroponics to  $1000 \text{ mg.L}^{-1}$  Ag-NPs or*  
359  *$1000 \text{ mg.L}^{-1}$   $\text{TiO}_2$ -NPs. Two color maps show Ag (A, C, I, K) or Ti (E, M) (red) superimposed to endogenous elements*  
360 *(S, P, K or Cl in green). Elemental distribution maps in temperature color for Ag (B, D, J, L), Ti (F, N), P (G) and Ca*  
361 *(H). Color bars represent the fluorescence counts. Maps were acquired on ID21 and LUCIA. Arrows indicate spots*  
362 *where  $\mu$ XANES spectra were recorded. For the figure in color, the reader is referred to the web version of this*  
363 *article.*

364





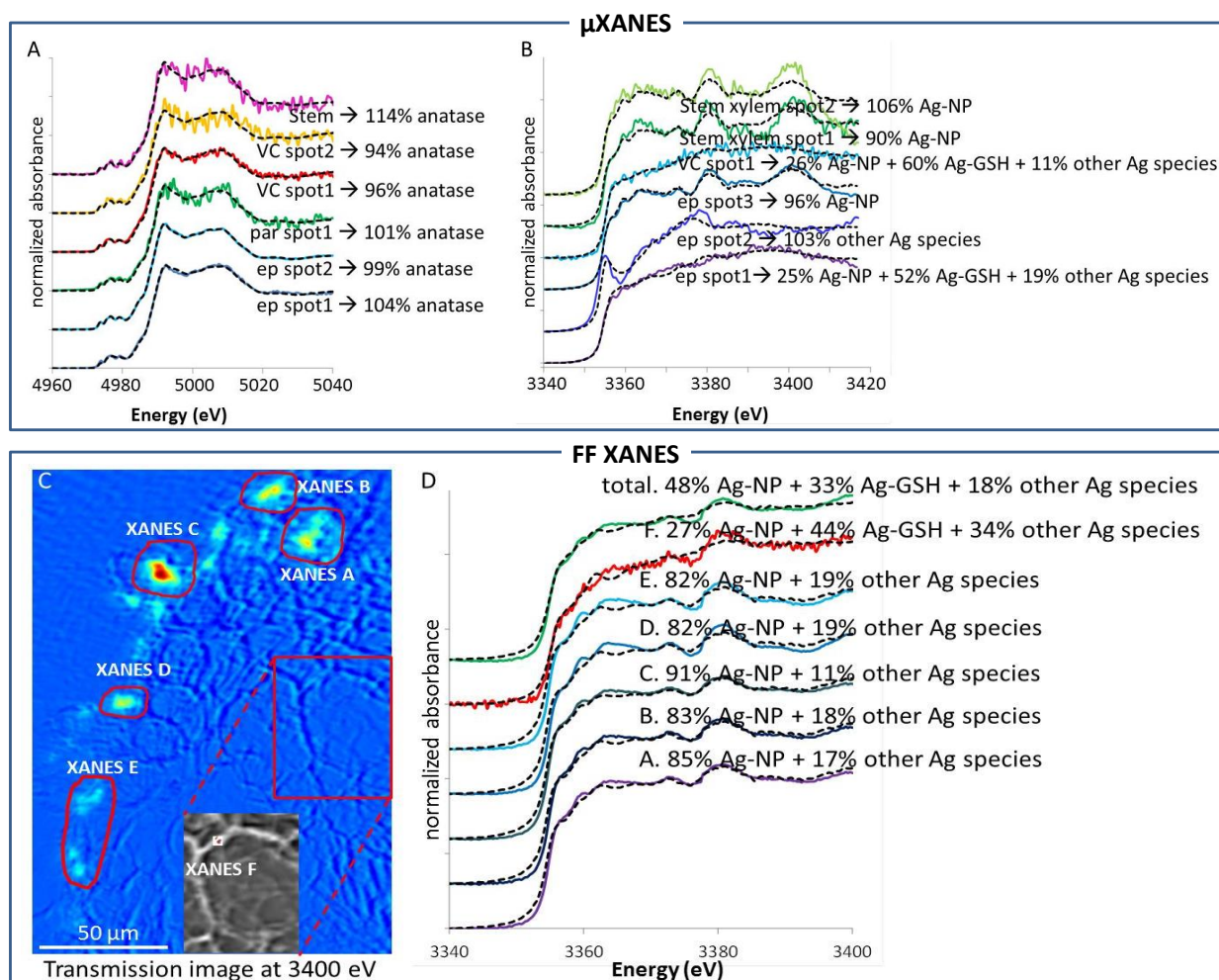
365

366

367 Metal speciation was determined from these maps (arrows in Figure 2 and data not shown) by  $\mu$ XANES  
 368 and using linear combination fitting of reference compounds (Table 1). Ti in the epidermis as well as in  
 369 the root parenchyma and vascular cylinder was present as anatase. It was also transferred to stems in  
 370 this chemical state (Figure 3A, Figure S9A, B - Appendix). The stability of anatase NPs in the plants is  
 371 consistent with previous publications [36,37,53,54]. Inversely, Ag was present in roots under two  
 372 oxidation states from 100%  $\text{Ag}^0$  to 100% monovalent Ag and in association with different ligands  
 373 regardless of the tissue (Figure 3B). The predominant ligand identified by linear combination fitting is  
 374 a thiol-containing molecule (glutathione). This molecule is known to be involved in plant detoxification  
 375 mechanisms and has been shown to increase in concentration in wheat exposed to Ag-NPs [55]. Ag-  
 376 thiol complexes have already been detected in lettuce leaves after foliar exposure to Ag-NPs [24]. Ag

377 in leaves was too diluted to obtain exploitable XANES spectra. Likewise, no good quality XANES spectra  
 378 could be obtained for roots exposed to lower NP concentrations (10 and 100 mg.L<sup>-1</sup>).

379  
 380 *Figure 3. XANES analysis in situ of Ti and Ag in root (VC: root vascular cylinder, par: root parenchyma, ep: root*  
 381 *epidermis) and stem cross-sections of lettuce in different acquisition modes:  $\mu$ XANES (Ti in A and Ag in B) and in*  
 382 *XANES full-field mode (transmission map of a root cross-section in C with selected area for XANES extraction,*  
 383 *corresponding spectra in D. “total” corresponds to all extractible spectra of the analyzed area). In plain lines*  
 384 *experimental data, in dotted lines the fit and reference compound contributions to the linear combination fits.*  
 385 *For the figure in color, the reader is referred to the web version of this article.*



386  
 387  
 388 To have a better understanding of Ag internalization mechanisms, a root cross-section was analyzed  
 389 by full-field XANES (Figure 3C, D, Table 1). This technique permits to obtain 2D speciation of an element

390 of interest over a large area but is restricted to samples with high concentrations of this element and  
 391 to thin cross-sections since the signal is recorded in transmission mode. At the moment this acquisition  
 392 mode runs at room temperature only, so root cross-sections were freeze-dried before analysis. The  
 393 overall signal of the root cross-section showed a contribution of three forms of Ag, half of the signal  
 394 came from Ag-NPs, and the other half from other Ag species with 33% being complexed by a thiol-  
 395 containing molecule. A spatial segregation seemed to exist between the epidermis and the  
 396 parenchyma. Indeed, Ag at the root surface showed only a moderate dissolution (between 10 and 20%)  
 397 whereas Ag in the parenchyma displayed a higher dissolution (78%, XANES F). These speciation results  
 398 corroborate the hypothesis stated after  $\mu$ PIXE/RBS analysis: Ag inside root tissue was mainly present  
 399 as monovalent Ag, with a small contribution from elemental Ag (as Ag-NPs). These results do not  
 400 permit to distinguish the two internalization scenarios stated before: only ions are internalized vs. Ag-  
 401 NPs are internalized and dissolved inside the cells. Indeed, plant exposure to ionic Ag also led to the  
 402 formation of Ag<sup>0</sup> in plant tissues [24,56,57]. Since TiO<sub>2</sub>-NPs can be internalized, it is conceivable that  
 403 Ag-NPs are internalized as well. Thus, the two pathways probably co-exist: both Ag ions and Ag-NPs  
 404 are taken up by roots, with later dissolution of Ag-NPs inside the tissue and resulting Ag<sup>+</sup> ions are partly  
 405 scavenged by the detoxification system. XANES analysis confirmed different behaviors for the two NPs:  
 406 Ti was detected in plant tissues as agglomerated but unchanged NPs, unlike Ag which was present as  
 407 Ag-NPs and secondary species including Ag<sup>+</sup> bound to thiol ligands.

408

409 Table 1: Summary of spectroscopic techniques employed in this study

Technique	Instrument	Information	Characteristics
$\mu$ XRF	Synchrotron (ID21 and LUCIA)	Distribution at the Ti K and Ag L edge	Very sensitive (1 $\mu$ g.g <sup>-1</sup> ) In association with $\mu$ XANES Cryogenic conditions
$\mu$ XRF	Synchrotron (ID22*)	Distribution at Ag K edge	K-edge more sensitive Better lateral resolution (sub-cellular scale) No information on light elements Freeze-dried samples
$\mu$ XANES	Synchrotron (ID21)	Speciation	<i>in situ</i> Cryogenic

Full-field XANES	Synchrotron (ID21)	Speciation	<i>in situ</i> Fast acquisition on large area Concentrated and thin samples (in transmission) Freeze-dried samples
$\mu$ PIXE/RBS	nuclear microprobe (AIFIRA)	Distribution + quantification	Sensitivity (100 $\mu\text{g}\cdot\text{g}^{-1}$ ) Local quantification For all elements (H $\rightarrow$ U) Freeze-dried samples

410 \* Since our experiment, ID22 nanoimaging beamline has been upgraded and relocated at ID16 (NINA).

411

## 412 **Conclusion**

413 This study highlights the interest of using spectroscopic beam-based techniques to analyze the fate of  
414 NPs in the environment and especially in biological matrixes. It permitted to bring new and original  
415 information that are mandatory for understanding the fate of NPs in plants, which are key information  
416 for risk assessment and food safety. For instance,  $\mu$ PIXE/RBS and  $\mu$ XRF showed that Ag-NPs were more  
417 efficiently taken up by roots than TiO<sub>2</sub>-NPs, whereas considering only ICP-MS/AES data, one could have  
418 had a reverse conclusion because of the presence of TiO<sub>2</sub>-NPs adsorbed on the root surface. Ag and Ti  
419 were observed in the stem, suggesting a transfer of the NPs and/or their secondary products to the  
420 edible parts of lettuce. The study of the speciation by XANES demonstrated different behaviors for  
421 those two NPs: Ti was detected in root tissues as agglomerated but unchanged NPs, unlike Ag which  
422 was present as Ag-NPs and secondary species including Ag<sup>+</sup> bound to thiol ligands. Another interesting  
423 piece of information is related to NP toxicity. In our exposure conditions, TiO<sub>2</sub>-NPs were not acutely  
424 toxic however, at high concentrations they had a clear impact on root homeostasis by disrupting Fe,  
425 Ca and P uptake which may lead to long-term toxicity. On the other hand, Ag-NPs were phytotoxic at  
426 all concentrations tested and altered to a higher extent root ionome. Obviously, those results have to  
427 be mitigated since exposure conditions are not representative of chronic contaminations. This  
428 represents the main limit of those techniques nowadays: their limit of detection which restricted, until  
429 recently, studies to exposure concentrations mimicking an acute contamination of the environment.  
430 Many other spectroscopic techniques exist that are equally useful and bring complementary data for  
431 instance at the sub-cellular level (nanoSIMS) or in depth profiling (ToF-SIMS) or on the bio-

432 macromolecule distribution ( $\mu$ FTIR). Finally coupling those spectroscopic methods with biochemical  
433 and molecular information would be a very powerful and promising approach in the future.

434

#### 435 **ACKNOWLEDGEMENTS**

436 The authors would like to thank the FP7 of the European Union for the funding (Nanohouse project  
437 no. 247810), the French program Equipex NanoID (ANR-10-EQPX-39-01), and French program LABEX  
438 Serenade (11-LABX-0064). Synchrotron experiments were performed on ID21 and ID22 beamlines at  
439 the European Synchrotron Radiation Facility (ESRF), Grenoble, France and on LUCIA beamline at SOLEIL  
440 (St Aubin, France). ISTERre is part of Labex OSUG@2020 (ANR10 LABX56). AIFIRA nuclear microprobe  
441 is also acknowledged for beamtime provision. The authors would like to thank Dr. Antoine Gehin for  
442 his precious help to prepare reference compounds in anoxic conditions for XANES experiment. The  
443 authors declare no competing financial interest.

444

#### 445 **APPENDIX A. SUPPLEMENTARY DATA**

446 Supplementary data to this article can be found online at doi:

447

448 **BIBLIOGRAPHY**

- 449 [1] www.nanotechproject.org, The project on emerging nanotechnologies, (2015).
- 450 [2] C. Kole, P. Kole, K.M. Randunu, P. Choudhary, R. Podila, P.C. Ke, et al., Nanobiotechnology can  
451 boost crop production and quality: first evidence from increased plant biomass, fruit yield and  
452 phytomedicine content in bitter melon (*Momordica charantia*), *BMC Biotechnol.* 13 (2013) 37–  
453 47. doi:10.1186/1472-6750-13-37.
- 454 [3] A. Massarsky, R. Abraham, K.C. Nguyen, P. Rippstein, A.F. Tayabali, V.L. Trudeau, et al.,  
455 Nanosilver cytotoxicity in rainbow trout (*Oncorhynchus mykiss*) erythrocytes and hepatocytes,  
456 *Comp. Biochem. Physiol. Part C Toxicol. Pharmacol.* 159 (2014) 10–21.  
457 doi:10.1016/j.cbpc.2013.09.008.
- 458 [4] S. Li, L.K. Wallis, H. Ma, S.A. Diamond, Phototoxicity of TiO<sub>2</sub> nanoparticles to a freshwater  
459 benthic amphipod: are benthic systems at risk?, *Sci Total Env.* 466-467 (2014) 800–808.  
460 doi:10.1016/j.scitotenv.2013.07.059.
- 461 [5] C. Larue, M. Pinault, B. Czarny, D. Georgin, D. Jaillard, N. Bendiab, et al., Quantitative evaluation  
462 of multi-walled carbon nanotube uptake in wheat and rapeseed, *J. Hazard. Mater.* 227 (2012)  
463 155–163. doi:10.1016/j.jhazmat.2012.05.033.
- 464 [6] J. Goldstein, D. Newbury, D. Joy, C. Lyman, P. Echlin, E. Lifshin, et al., *Scanning Electron  
465 Microscopy and X-ray Microanalysis*, Springer, 2003.
- 466 [7] E. Bigorgne, L. Foucaud, E. Lapied, J. Labille, C. Botta, C. Sirguy, et al., Ecotoxicological  
467 assessment of TiO<sub>2</sub> byproducts on the earthworm *Eisenia fetida*, *Env. Pollut.* 159 (2011) 2698–  
468 2705. doi:10.1016/j.envpol.2011.05.024.
- 469 [8] D. Cleveland, S.E. Long, P.L. Pennington, E. Cooper, M.H. Fulton, G.I. Scott, et al., Pilot estuarine  
470 mesocosm study on the environmental fate of silver nanomaterials leached from consumer  
471 products, *Sci Total Env.* 421-422 (2012) 267–272. doi:10.1016/j.scitotenv.2012.01.025.
- 472 [9] R. Kaveh, Y.S. Li, S. Ranjbar, R. Tehrani, C.L. Brueck, B. Van Aken, Changes in *Arabidopsis*  
473 *thaliana* gene expression in response to silver nanoparticles and silver ions, *Env. Sci Technol.* 47  
474 (2013) 10637–10644. doi:10.1021/es402209w.
- 475 [10] C. Mariet, O. Belhadj, S. Leroy, F. Carrot, N. Metrich, Relevance of NH<sub>4</sub>F in acid digestion before  
476 ICP-MS analysis, *Talanta.* 77 (2008) 445–450.
- 477 [11] E. Donner, T. Punshon, M.L. Guerinot, E. Lombi, Functional characterisation of metal(loid)  
478 processes in planta through the integration of synchrotron techniques and plant molecular  
479 biology, *Anal. Bioanal. Chem.* 402 (2012) 3287–3298. doi:10.1007/s00216-011-5624-9.
- 480 [12] G. Sarret, E. Pilon-Smits, H. Castillo-Michel, M. Isaure, F.J. Zhao, R. Tappero, Use of synchrotron-  
481 based techniques to elucidate metal uptake and metabolism in plants, in: D.L. Sparks (Ed.), *Adv.  
482 Agonomy*, Academic Press, 2013: pp. 1–82.
- 483 [13] B. Wang, Z. Wang, W. Feng, M. Wang, Z. Hu, Z. Chai, et al., New methods for nanotoxicology:  
484 synchrotron radiation-based techniques, *Anal. Bioanal. Chem.* 398 (2010) 667–676.  
485 doi:10.1007/s00216-010-3752-2.
- 486 [14] G.E. Schaumann, A. Philippe, M. Bundschuh, G. Metreveli, S. Klitzke, D. Rakcheev, et al.,  
487 Understanding the fate and biological effects of Ag- and TiO<sub>2</sub>-nanoparticles in the environment:  
488 The quest for advanced analytics and interdisciplinary concepts, *Sci. Total Environ.* 535 (2014)  
489 3–19. doi:10.1016/j.scitotenv.2014.10.035.
- 490 [15] A. Gogos, K. Knauer, T.D. Bucheli, Nanomaterials in plant protection and fertilization: current  
491 state, foreseen applications, and research priorities, *J. Agric. Food Chem.* 60 (2012) 9781–9792.  
492 doi:10.1021/jf302154y.
- 493 [16] A.G. Kachenko, R. Siegele, N.P. Bhatia, B. Singh, M. Ionescu, Evaluation of specimen preparation  
494 techniques for micro-PIXE localisation of elements in hyperaccumulating plants, *Nucl. Instrum.  
495 Methods Phys. Res. Sect. B Beam Interact. Mater. At.* 266 (2008) 1598–1604.  
496 doi:10.1016/j.nimb.2007.11.017.

- 497 [17] S. Sorieul, P. Alfaut, L. Daudin, L. Serani, P. Moretto, Aifira: An ion beam facility for  
498 multidisciplinary research, *Nucl. Instrum. Methods Phys. Res. Sect. B Beam Interact. Mater. At.*  
499 332 (2014) 68–73. doi:10.1016/j.nimb.2014.02.032.
- 500 [18] BARBOTTEAU Software Informer: Latest BARBOTTEAU software updates and reviews:  
501 SupaVISIO, etc., (n.d.). <http://barbotteau.software.informer.com/> (accessed September 28,  
502 2015).
- 503 [19] M. Mayer, SIMNRA, a simulation program for the analysis of NRA, RBS and ERDA, in: J.L.  
504 Duggan, I.L. Morgan (Eds.), *Appl. Accel. Res. Ind. Pts 1 2*, Amer Inst Physics, Melville, 1999: pp.  
505 541–544. doi:10.1016/S00081503200132.
- 506 [20] J.L. Campbell, T.L. Hopman, J.A. Maxwell, Z. Nejedly, The Guelph PIXE software package III:  
507 Alternative proton database, *Nucl. Instrum. Methods Phys. Res. Sect. B-Beam Interact. Mater.*  
508 *At.* 170 (2000) 193–204. doi:10.1016/S0168-583X(00)00156-7.
- 509 [21] M. Salomé, M. Cotte, R. Baker, R. Barrett, N. Benseny-Cases, G. Berruyer, et al., The ID21  
510 Scanning X-ray Microscope at ESRF, *J. Phys. Conf. Ser.* 425 (2013) 182004.
- 511 [22] G. Martínez-Criado, R. Tucoulou, P. Cloetens, P. Bleuet, S. Bohic, J. Cauzid, et al., Status of the  
512 hard X-ray microprobe beamline ID22 of the European Synchrotron Radiation Facility, *J.*  
513 *Synchrotron Radiat.* 19 (2012) 10–18. doi:10.1107/S090904951104249X.
- 514 [23] V.A. Sole, E. Papillon, M. Cotte, P. Walter, J. Susini, A multiplatform code for the analysis of  
515 energy-dispersive X-ray fluorescence spectra, *Spectrochim. Acta Part B-At. Spectrosc.* 62 (2007)  
516 63–68. doi:10.1016/j.sab.2006.12.002.
- 517 [24] C. Larue, H. Castillo-Michel, S. Sobanska, L. Cécillon, S. Bureau, V. Barthès, et al., Foliar exposure  
518 of the crop *Lactuca sativa* to silver nanoparticles: Evidence for internalization and changes in Ag  
519 speciation, *J. Hazard. Mater.* 264 (2014) 98–106. doi:10.1016/j.jhazmat.2013.10.053.
- 520 [25] C. Larue, H. Castillo-Michel, S. Sobanska, N. Trcera, S. Sorieul, L. Cécillon, et al., Fate of pristine  
521 TiO<sub>2</sub> nanoparticles and aged paint-containing TiO<sub>2</sub> nanoparticles in lettuce crop after foliar  
522 exposure, *J Hazard Mater.* 273 (2014) 17–26. doi:10.1016/j.jhazmat.2014.03.014.
- 523 [26] B. Fayard, E. Pouyet, G. Berruyer, D. Bugnazet, C. Cornu, M. Cotte, et al., The new ID21 XANES  
524 full-field end-station at ESRF, *J. Phys. Conf. Ser.* 425 (2013) 192001.
- 525 [27] P. Paleo, E. Pouyet, J. Kieffer, Image stack alignment in full-field X-ray absorption spectroscopy  
526 using SIFT\_PyOCL, *J. Synchrotron Radiat.* 21 (2014) 456–461. doi:10.1107/S160057751400023X.
- 527 [28] Y. Liu, F. Meirer, P.A. Williams, J. Wang, J.C. Andrews, P. Pianetta, TXM-Wizard: a program for  
528 advanced data collection and evaluation in full-field transmission X-ray microscopy, *J.*  
529 *Synchrotron Radiat.* 19 (2012) 281–287. doi:10.1107/S0909049511049144.
- 530 [29] Ravel, Newville, ATHENA, ARTEMIS, HEPHAESTUS: data analysis for X-ray absorption  
531 spectroscopy using IFEFFIT, *J. Synchrotron Radiat.* 12 (2005) 537–541.  
532 doi:10.1107/S0909049505012719.
- 533 [30] R Core Team, R: A language and environment for statistical computing, (2015). [http://www.R-](http://www.R-project.org/)  
534 [project.org/](http://www.R-project.org/).
- 535 [31] J. Oksanen, F.G. Blanchet, R. Kindt, P. Legendre, P.R. Minchin, R.B. O’Hara, et al., *vegan*:  
536 *Community Ecology Package*. R package version 2.2-1., (2015). [http://CRAN.R-](http://CRAN.R-project.org/package=vegan)  
537 [project.org/package=vegan](http://CRAN.R-project.org/package=vegan).
- 538 [32] W.N. Venables, B.D. Ripley, *Modern Applied Statistics with R*, Fourth, Springer, New York, 2002.
- 539 [33] E. Seeger, A. Baun, M. Kastner, S. Trapp, Insignificant acute toxicity of TiO<sub>2</sub> nanoparticles to  
540 willow trees, *J. Soils Sediments.* 9 (2009) 46–53. doi:10.1007/s11368-008-0034-0.
- 541 [34] D.L. Jacob, J.D. Borchardt, L. Navaratnam, M.L. Otte, A.N. Bezbaruah, Uptake and translocation  
542 of Ti from nanoparticles in crops and wetland plants, *Int J Phytoremediation.* 15 (2013) 142–53.  
543 doi:10.1080/15226514.2012.683209.
- 544 [35] A.S. Foltete, J.F. Masfaraud, E. Bigorgne, J. Nahmani, P. Chaurand, C. Botta, et al.,  
545 Environmental impact of sunscreen nanomaterials: ecotoxicity and genotoxicity of altered TiO<sub>2</sub>  
546 nanocomposites on *Vicia faba*, *Env. Pollut.* 159 (2011) 2515–22.  
547 doi:10.1016/j.envpol.2011.06.020.

- 548 [36] C. Larue, J. Laurette, N. Herlin-Boime, H. Khodja, B. Fayard, A.M. Flank, et al., Accumulation,  
549 translocation and impact of TiO<sub>2</sub> nanoparticles in wheat (*Triticum aestivum* spp.): influence of  
550 diameter and crystal phase, *Sci Total Env.* 431 (2012) 197–208.  
551 doi:10.1016/j.scitotenv.2012.04.073.
- 552 [37] C. Larue, G. Veronesi, A.M. Flank, S. Surble, N. Herlin-Boime, M. Carriere, Comparative uptake  
553 and impact of TiO<sub>2</sub> nanoparticles in wheat and rapeseed, *J Toxicol Env. Health A.* 75 (2012)  
554 722–734. doi:10.1080/15287394.2012.689800.
- 555 [38] P. Thuesombat, S. Hannongbua, S. Akasit, S. Chadchawan, Effect of silver nanoparticles on rice  
556 (*Oryza sativa* L. cv. KDML 105) seed germination and seedling growth, *Ecotoxicol. Environ. Saf.*  
557 104 (2014) 302–309. doi:10.1016/j.ecoenv.2014.03.022.
- 558 [39] L.Y. Yin, Y.W. Cheng, B. Espinasse, B.P. Colman, M. Auffan, M. Wiesner, et al., More than the  
559 ions: The Effects of Silver Nanoparticles on *Lolium multiflorum*, *Environ. Sci. Technol.* 45 (2011)  
560 2360–2367. doi:10.1021/es103995x.
- 561 [40] U. Song, H. Jun, B. Waldman, J. Roh, Y. Kim, J. Yi, et al., Functional analyses of nanoparticle  
562 toxicity: a comparative study of the effects of TiO<sub>2</sub> and Ag on tomatoes (*Lycopersicon*  
563 *esculentum*), *Ecotoxicol. Environ. Saf.* 93 (2013) 60–67. doi:10.1016/j.ecoenv.2013.03.033.
- 564 [41] D.A. Notter, D.M. Mitrano, B. Nowack, Are nanosized or dissolved metals more toxic in the  
565 environment? A meta-analysis, *Environ. Toxicol. Chem. SETAC.* 33 (2014) 2733–2739.  
566 doi:10.1002/etc.2732.
- 567 [42] E. Navarro, F. Piccapietra, B. Wagner, F. Marconi, R. Kaegi, N. Odzak, et al., Toxicity of silver  
568 nanoparticles to *Chlamydomonas reinhardtii*, *Environ. Sci. Technol.* 42 (2008) 8959–8964.  
569 doi:10.1021/es801785m.
- 570 [43] A.G. González, S. Mombo, J. Leflaive, A. Lamy, O.S. Pokrovsky, J.-L. Rols, Silver nanoparticles  
571 impact phototrophic biofilm communities to a considerably higher degree than ionic silver,  
572 *Environ. Sci. Pollut. Res. Int.* 22 (2015) 8412–8424. doi:10.1007/s11356-014-3978-1.
- 573 [44] C. Beer, R. Foldbjerg, Y. Hayashi, D.S. Sutherland, H. Autrup, Toxicity of silver nanoparticles -  
574 nanoparticle or silver ion?, *Toxicol. Lett.* 208 (2012) 286–292. doi:10.1016/j.toxlet.2011.11.002.
- 575 [45] N. Lubick, Nanosilver toxicity: ions, nanoparticles--or both?, *Environ. Sci. Technol.* 42 (2008)  
576 8617–8617. doi:10.1021/es8026314.
- 577 [46] D. McShan, P.C. Ray, H. Yu, Molecular toxicity mechanism of nanosilver, *J. Food Drug Anal.* 22  
578 (2014) 116–127. doi:10.1016/j.jfda.2014.01.010.
- 579 [47] M. Khodakovskaya, E. Dervishi, M. Mahmood, Y. Xu, Z.R. Li, F. Watanabe, et al., Carbon  
580 nanotubes are able to penetrate plant seed coat and dramatically affect seed germination and  
581 plant growth, *Acs Nano.* 3 (2009) 3221–3227. doi:10.1021/nn900887m.
- 582 [48] S. Leclerc, K.J. Wilkinson, Bioaccumulation of Nanosilver by *Chlamydomonas reinhardtii*-  
583 nanoparticle or the free ion?, *Environ. Sci. Technol.* 48 (2014) 358–364. doi:10.1021/es404037z.
- 584 [49] D.E. Salt, I. Baxter, B. Lahner, Ionomics and the Study of the Plant Ionome, *Annu. Rev. Plant*  
585 *Biol.* 59 (2008) 709–733. doi:10.1146/annurev.arplant.59.032607.092942.
- 586 [50] H. Qian, X. Peng, X. Han, J. Ren, L. Sun, Z. Fu, Comparison of the toxicity of silver nanoparticles  
587 and silver ions on the growth of terrestrial plant model *Arabidopsis thaliana*, *J. Environ. Sci.*  
588 *China.* 25 (2013) 1947–1955. doi:10.1016/S1001-0742(12)60301-5.
- 589 [51] K. Varmuza, P. Filzmoser, *Introduction to Multivariate Statistical Analysis in Chemometrics*, CRC  
590 Press, 2009.
- 591 [52] R. Rousseau, Detection limit and estimate of uncertainty of analytical XRF results, *Rigaku J.* 18  
592 (2001) 33–47.
- 593 [53] A.D. Servin, H. Castillo-Michel, J.A. Hernandez-Viezcas, B.C. Diaz, J.R. Peralta-Videa, J.L. Gardea-  
594 Torresdey, Synchrotron Micro-XRF and Micro-XANES Confirmation of the Uptake and  
595 Translocation of TiO<sub>2</sub> Nanoparticles in Cucumber (*Cucumis sativus*) Plants, *Environ. Sci.*  
596 *Technol.* 46 (2012) 7637–7643. doi:10.1021/es300955b.
- 597 [54] A.D. Servin, M.I. Morales, H. Castillo-Michel, J.A. Hernandez-Viezcas, B. Munoz, L. Zhao, et al.,  
598 Synchrotron verification of TiO<sub>2</sub> accumulation in cucumber fruit: a possible pathway of TiO<sub>2</sub>



- 599 nanoparticle transfer from soil into the food chain, *Env. Sci Technol.* 47 (2013) 11592–11598.  
600 doi:10.1021/es403368j.
- 601 [55] C.O. Dimkpa, J.E. McLean, N. Martineau, D.W. Britt, R. Haverkamp, A.J. Anderson, Silver  
602 nanoparticles disrupt wheat (*Triticum aestivum* L.) growth in a sand matrix, *Env. Sci Technol.* 47  
603 (2013) 1082–1090. doi:10.1021/es302973y.
- 604 [56] R.G. Haverkamp, A.T. Marshall, The mechanism of metal nanoparticle formation in plants: limits  
605 on accumulation, *J. Nanoparticle Res.* 11 (2009) 1453–1463. doi:10.1007/s11051-008-9533-6.
- 606 [57] J.L. Gardea-Torresdey, E. Gomez, J.R. Peralta-Videa, J.G. Parsons, H. Troiani, M. Jose-Yacaman,  
607 Alfalfa Sprouts: A Natural Source for the Synthesis of Silver Nanoparticles, *Langmuir.* 19 (2003)  
608 1357–1361. doi:10.1021/la020835i.  
609